Estimation of Stratospheric Flow from Satellite 15-Micron Radiation[1,2]

J. ALLEN ZAK[3] AND H. A. PANOFSKY

Pennsylvania State University, University Park

(Manuscript received 14 September 1967)

ABSTRACT

Ten-day average "thermal winds" derived from TIROS VII in the CO_2 band are compared to the corresponding geostrophic winds at 10 mb at latitudes 40–60N. The correlations for the west-east components are of order 0.8, those for the south-north components, 0.5. Much of the correlation in the U components is due to concurrent seasonal trend.

1. Introduction

TIROS VII and Nimbus II carried out radiation experiments in wavelength intervals near 15 μ, the location of the CO_2 band. The radiation amount received in this wavelength interval depends almost entirely on the temperature distribution in the stratosphere. Conversely, stratospheric characteristics can be inferred from satellite data at these wavelengths.

The sensor in Nimbus II functioned only during a few summer months when the northern stratosphere is relatively uninteresting; in the Southern Hemisphere, stratospheric data are too spotty to make a meaningful comparison between them and satellite data. Also, the Nimbus window was relatively wide, causing some contamination from high clouds in the troposphere.

TIROS VII, however, operated satisfactorily for over a year. The main disadvantage of its CO_2 channel (channel 1) was that it was plagued by random errors. In order to reduce the effect of these errors, Kennedy (1966) computed 15-μ radiation amounts for 10-day average periods and constructed Northern Hemisphere isopleths from them. Because stratospheric movements are generally slow, such isopleths should reflect the most important stratospheric developments.

Even casual inspection shows that the isopleths on Kennedy's charts behave quite similarly to the contour lines on 10-mb charts at high latitudes. It thus appears possible to infer geostrophic winds at 10-mb from CO_2 band isopleths. This paper presents some statistics of the relationship between Kennedy's 10-day mean radiation data and 10-mb, 10-day mean geostrophic winds computed from the charts analyzed under the direction of Scherhag (1963, 1964).

[1] Contribution No. 67–13, Earth and Mineral Sciences Experiment Station, Pennsylvania State University.

[2] The views expressed herein are those of the author and do not necessarily reflect the views of the U. S. Air Force or the Department of Defense.

[3] Permanent affiliation: Air Weather Service, U. S. Air Force.

2. Theory

Kennedy's charts actually present the radiation data in terms of equivalent black-body temperatures. The radiance received is related to these black-body temperatures T_b by

$$I=\int_0^\infty \phi_\lambda B_\lambda(T_b)d\lambda. \tag{1}$$

Here, B_λ is the Planck function and ϕ_λ the rather narrow filter function used in the receiver. Because the spectral window is so narrow, Eq. (1) can be approximated by

$$I=A\overline{B_\lambda(T_b)}, \tag{2}$$

where A is the integral over the filter function and $\bar{B}$ is the Planck relation averaged over the spectral window.

According to Nordberg *et al.* (1965), the radiance received by the satellite is given by

$$I=\int_0^\infty\int_0^\infty \phi_\lambda B_\lambda(T)\frac{\partial\tau_\lambda}{\partial h}d\lambda\,dh, \tag{3}$$

where τ_λ is the atmospheric transmissivity, and h is height.

If we equate (2) and (3), we obtain

$$\overline{B_\lambda(T_b)}=\frac{1}{A}\int_0^\infty \overline{B_\lambda(T)}\int_0^\infty \phi_\lambda\frac{\partial\tau_\lambda}{\partial h}d\lambda\,dh. \tag{4}$$

We now take the isobaric gradient of Eq. (4) and introduce the thermal wind equation on the right to obtain

$$\nabla_p T_b=\frac{f\bar{T}}{g_0}\int_0^\infty W(h)\frac{\partial \mathbf{V}}{\partial h}\times\mathbf{k}\,dh, \tag{5}$$

where $W(h)$ can be regarded as a weight function for the

vertical wind shear. It is defined by

$$W(h)=\frac{1}{A}\frac{d\overline{B_\lambda(T)}}{dT}\int_0^\infty \frac{\partial \tau_\lambda}{\partial h}\phi_\lambda d\lambda \Big/ \frac{d\overline{B_\lambda(T_b)}}{dT_b}. \quad (6)$$

Since $W(h)$ vanishes at small and large h, integration by parts leads to

$$\nabla_p T_b=-\frac{f\bar{T}}{g_0}\int_0^\infty \frac{\partial W}{\partial h}(\mathbf{V}\times\mathbf{k})dh, \quad (7)$$

where g_0 is standard gravity and f the Coriolis parameter. We now divide the integral in Eq. (7) into two parts, one below H and the other above H, where H is the level of maximum W, or approximately 25 km. Because $\partial W/\partial h$ is positive below H and negative above, we may now write

$$\nabla_p T_b=\frac{f\bar{T}}{g_0}\left[\int_H^\infty \left|\frac{\partial W}{\partial h}\right|(\mathbf{V}\times\mathbf{k})dh-\int_0^H \left|\frac{\partial W}{\partial h}\right|(\mathbf{V}\times\mathbf{k})dh\right]. \quad (8)$$

Thus, the vector gradient of black-body temperatures as determined from Kennedy's charts can be regarded as representing the difference between two weighted mean winds, one above H, the other below. The weighting function is in each case $|\partial W/\partial h|$. Fig. 1 shows this weighting function as derived from Bandeen's transmissivities (1963) for zero nadir angle and the Planck functions for typical temperatures occurring at the various levels. The derivative $d\overline{B_\lambda(T_b)}/dT_b$ was evaluated for a temperature of 235K.

The figure shows that winds at levels as high as 50–60 km influence the isobaric gradient on Kennedy's maps. Since the fastest winds of all are found at these altitudes, the sign and magnitude of the weighted vector differences are largely determined by the winds in the upper stratosphere. For larger nadir angles, the curve has to be raised a few kilometers so that even winds in the lowest mesosphere exert some influence on the weighted wind difference.

It is difficult to test Eq. (8) directly on the basis of Kennedy's maps because they represent 10-day averages for nadir angles of 0–40°. Nevertheless, a partial test was attempted for three of Kennedy's charts when rocket ascents were available at Wallops Island, Va., for 2–4 days in or near the 10-day period covered by Kennedy's charts. The particulars are given in Table 2.

TABLE 1. Temperature gradients calculated from wind profile-weighting function products and those measured from charts of T_b.

Wind profile time period	Satellite T_b time period	Calculated temperature gradient	Satellite temperature gradient
1, 8, 13 Nov. 1963	7–16 Nov. 1963	1K(1739 km)$^{-1}$	1K(925 km)$^{-1}$
31 Jan., 4, 5, 7 Feb. 1964	31 Jan.–9 Feb. 1964	1K(2118 km)$^{-1}$	1K(647 km)$^{-1}$
20, 25 Mar. 1964	18–27 Mar. 1964	−1K(127 km)$^{-1}$	−1K(370 km)$^{-1}$

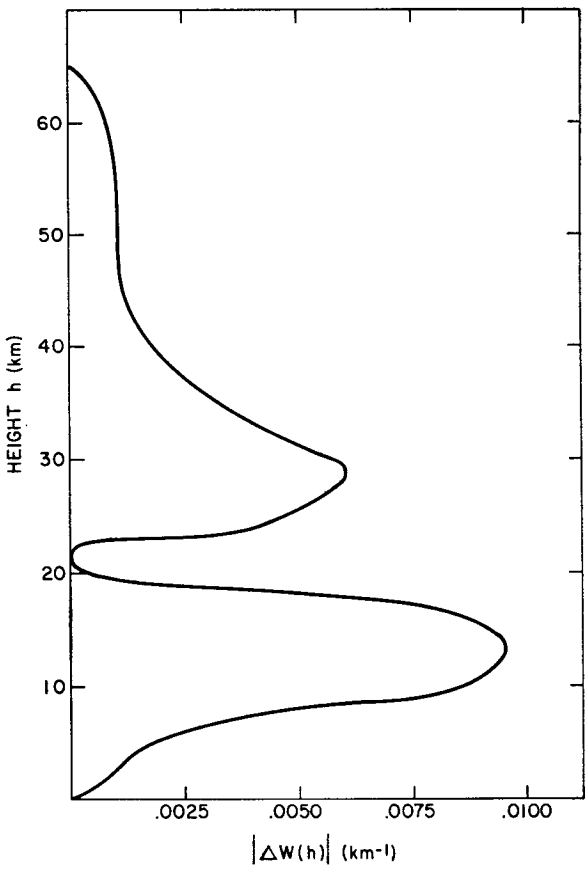

FIG. 1. Change in absolute value of the weighting function $W(h)$ computed for 2½-km height intervals.

The rocket data were taken from Meteorological Rocket Network Committee tabulations.

Apparently the north-south temperature gradients calculated from the weighting function of Fig. 1 have the right sign and order of magnitude. Better agreement would be expected only if true 10-day wind averages could have been computed.

3. Satellite temperature and 10-mb winds

The 10-mb surface is located at the highest level for which daily isobaric charts (constructed in Berlin) were available during the period of activity of TIROS VII. From these, 10-day average geostrophic winds could be obtained and compared with the temperature gradients taken from Kennedy's charts. The reason why a fairly high correlation was expected between these two quantities is that, as we have seen, the satellite temperature gradient vector is dominated in direction and magnitude by the winds in the upper stratosphere above 25 km and even the lowest mesosphere. Further, the average wind vector between 25 and 60 km tends to be in the same direction as the wind vector at 30 km, and its speed tends to be proportional. These characteristics appear to be best preserved at latitudes 40° and further

TABLE 2. Documentation data concerning 15-μ charts used [after Kennedy (1966)].

Dates (incl.)	Regular (dependent) data FMRT reels	Orbits (incl.)	Total no. of orbits
30 Sep.–9 Oct. 63	437–446	1517–1655	61
19 Oct.–28 Oct. 63	456–465	1794–1933	58
29 Oct.–7 Nov. 63	466–475	1940–2094	57
17 Nov.–27 Nov. 63	485–495	2234–2379	55
1 Dec.–10 Dec. 63	496–505	2437–2575	37
22 Dec.–31 Dec. 63	515–525	2743–2891	43
2 Jan.–11 Jan. 64	526–536	2909–3055	52
20 Jan.–29 Jan. 64	545–554	3181–3314	66
31 Jan.–9 Feb. 64	555–564	3341–3475	63
19 Feb.–28 Feb. 64	574–583	3620–3757	49
28 Feb.–8 Mar. 64	583–592	3750–3888	43
18 Mar.–27 Mar. 64	602–611	4027–4165	64
1 Apr.–10 Apr. 64	617–626	4246–4384	61
10 Oct.–19 Oct. 63	437–456	1664–1801	56
7 Nov.–16 Nov. 63	475–484	2086–2225	42
10 Dec.–19 Dec. 63	505–514	2568–2706	48
11 Jan.–20 Jan. 64	536–545	3050–3187	46
9 Feb.–18 Feb. 64	564–573	3472–3611	67
9 Mar.–18 Mar. 64	593–602	3896–4033	55

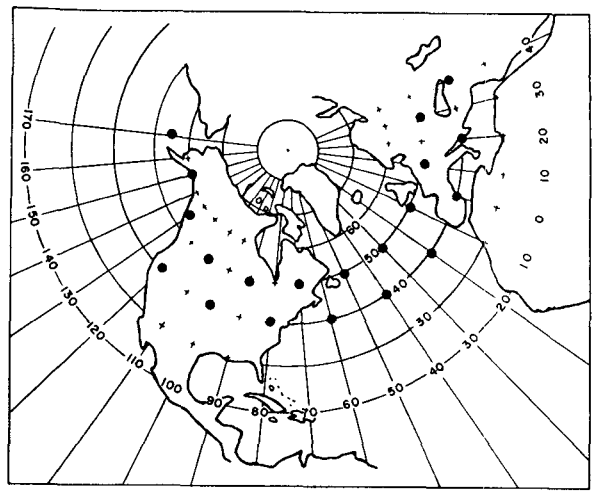

FIG. 2. Grid points used in this study.

north; hence, the comparison of satellite temperature gradients with 10-mb contour gradients was confined to these latitudes.

Fig. 2 shows the grid points used in the comparison, mostly at latitudes 40 and 50N where the observations were judged to be sufficient to estimate reasonably accurate 10-day mean, 10-mb contour gradients and satellite temperature gradients. Table 2 gives the particulars concerning dates and orbits used. Note that statistics were first computed only from thirteen 10-day periods; observations during additional periods were processed independently as a check on the statistics obtained from the first set of data.

The comparison between the two sets of charts was actually made in terms of "winds" in knots. East-west and north-south geostrophic wind components were evaluated from the 10-mb charts. Fictitious "wind" components were computed from Kennedy's charts through the formulas

$$U=-\frac{R}{f}\ln\left(\frac{100\text{ mb}}{10\text{ mb}}\right)\frac{\partial T_b}{\partial y}, \tag{9}$$

$$V=\frac{R}{f}\ln\left(\frac{100\text{ mb}}{10\text{ mb}}\right)\frac{\partial T_b}{\partial x}. \tag{10}$$

Here R is the gas constant for dry air and U and V represent wind components in the x direction (east) and y direction (north), respectively. These quantities would represent thermal wind components between 10 and 100 mb if Kennedy's black-body temperatures represented mean temperatures in that layer. As it is, these thermal winds are proportional, but not equal, to the x component and y component of the quantity on the right of Eq. (8). In general, all data were obtained for all grid points of Fig. 2 during all 19 periods. Only an apparent singularity in the field of T_b during the first 10

TABLE 3. Summary of statistical results.

Location component	All latitudes U	All latitudes V	50, 55, 60N U	50, 55, 60N V	40N U	40N V
			Regular (dependent) data			
Standard deviation (kt) Sat.	33.1	15.0	35.1	16.4	30.2	12.6
Standard deviation (kt) 10 mb	41.5	11.9	47.1	12.8	33.5	9.7
Observation no.	257	257	141	141	116	116
Correlation coefficient	0.834	0.465	0.840	0.463	0.830	0.379
Scatter (kt)	23.0	10.6	25.6	11.3	18.7	9.0
			Independent data			
Standard deviation (kt) Sat.	28.1	17.2	30.6	20.2	24.7	12.0
Standard deviation (kt) 10 mb	38.0	17.7	39.5	20.7	36.4	11.4
Observation no.	120	120	66	66	54	54
Correlation coefficient	0.775	0.587	0.813	0.594	0.716	0.482
Scatter (kt)	24.1	14.3	22.9	16.7	25.4	10.0
Scatter of independent data about line of regression from dependent data (kt)	25.4	15.0	24.1	18.0	26.8	10.1

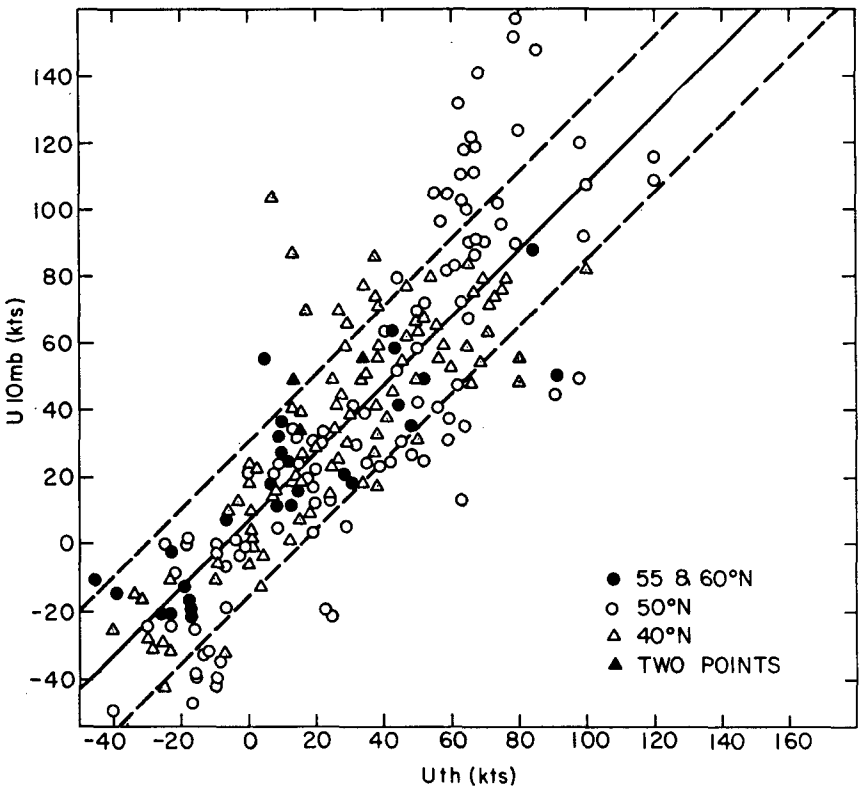

FIG. 3. Satellite thermal wind as a function of 10-mb geostrophic wind for U components. Points represent 10-day averages for the grid shown in Fig. 5 during the period from October 1963 to April 1964. Linear regression line and scatter are shown

days of April over the Gulf of St. Lawrence was judged to be unreal and was omitted.

Table 3 gives the results of the statistical comparison between 10-mb and satellite data. The observations are also graphically presented in Figs. 3 and 4.

It is clear from the statistics in Table 3 that the correlations between the corresponding east-west U components are generally large, varying from 0.72 to 0.84 for the various categories. These large correlations are produced to a considerable extent by the large seasonal

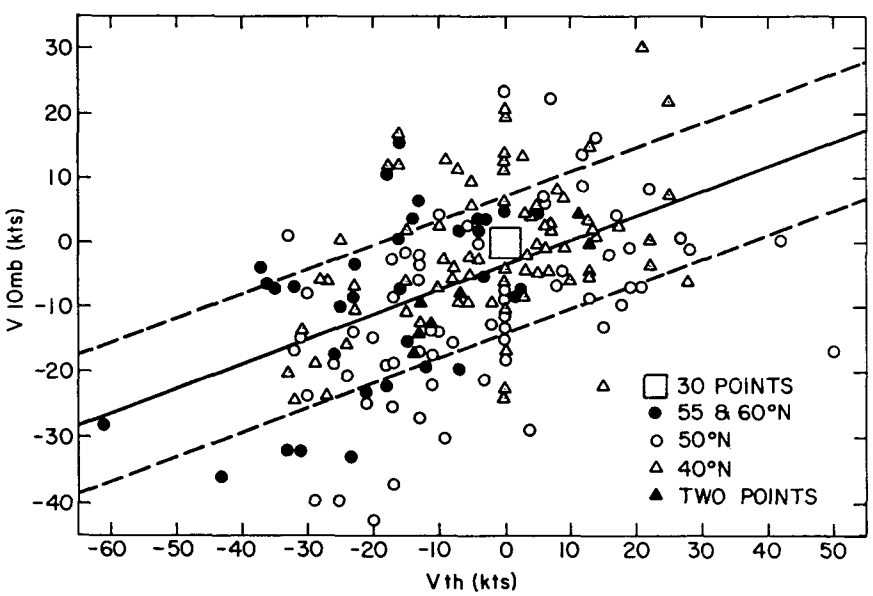

FIG. 4. Same as Fig. 3 for V components.

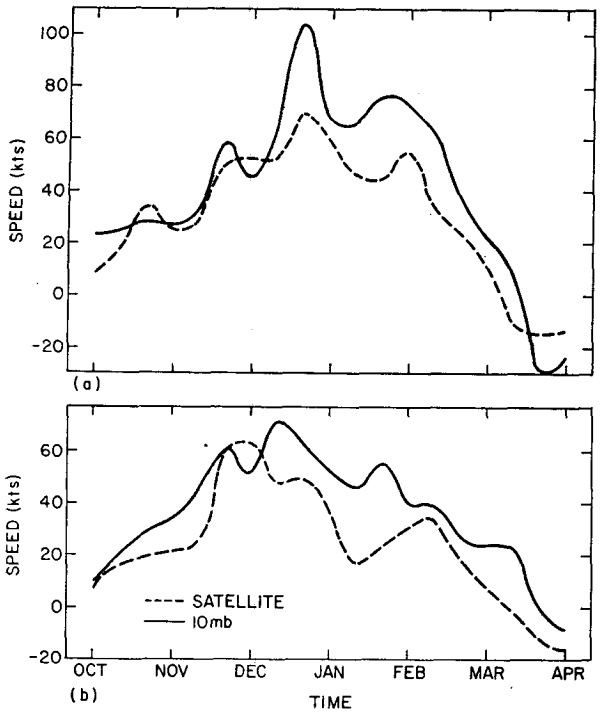

FIG. 5. Seasonal variation of the 10-day mean zonal component of the satellite thermal wind and observed 10-mb wind for (a) 50–60N averaged for all longitudes from 170W to 30E; (b) 40N averaged for all longitudes from 120W to 40E.

variation of the U components throughout the period of analysis, from strong westerly components at the beginning to weak easterlies at the end. This seasonal variation will be described in detail later. For any given month, the correlation would be much smaller.

There is no such general trend in the V-components so that here the correlations are smaller, though still significantly positive, varying from 0.59 to 0.38. This difference in the trends of the U and the V components is also brought out by the fact that the standard deviations are significantly larger for the U components.

Thus, we are led to the result that, in spite of the lower correlations, the scatter of the V components about their lines of regressions is smaller than that of the U components about their lines of regression. In other words, the error of estimate of the 10-mb U components from satellite data in knots is much larger than the error of estimate of the V's.

The last line in Table 3 presents the error in estimation of the wind components in the test sample from the regression line of the developmental sample.

Fig. 5 further illustrates the seasonal trends in the U components of the 10-mb winds and in the satellite winds. The vertical scale in the satellite winds is arbitrary. Clearly, there are strong seasonal variations in both variables, and they are quite well correlated with each other. At the higher latitude, even the fluctuations with periods of the order of a month appear to be in phase. The figure also suggests that the changeover from westerlies to easterlies at 10-mb in spring can be estimated from the satellite data to within about 10 days or less.

In summary, broad-band satellite data near 10 μ give useful information about the circulation in the middle stratosphere. It may be possible to apply the results to an estimation of the stratospheric circulation in middle latitudes in the Southern Hemisphere in its winter from the radiation recorded by Nimbus II.

Acknowledgments. The authors would like to express their appreciation to Mr. William Bandeen of NASA for many frutiful discussions, and to Dr. A. K. Blackadar for reading the manuscript.

REFERENCES

Bandeen, W. R., *et al.*, 1963: Experimental confirmation from the TIROS VII meteorological satellite of the theoretically calculated radiance of the earth within the 15-micron band of carbon dioxide. *J. Atmos. Sci.*, **19**, 52–55.

Kennedy, James S., 1966: An atlas of stratospheric mean isotherms derived from TIROS VII observations. Goddard Space Flight Center, NASA, X-620-67-134, 37 pp.

Nordberg, W., *et al.*, 1965: Stratospheric temperature patterns based on radiometric measurements from the TIROS VII satellite. NASA TN D-2798, 12–36.

Scherhag, R., *et al.*, 1963, 1964: Daily and monthly Northern Hemispheric 10-millibar synoptic weather maps. Inst. für Meteorologie und Geophysik der freien Universität Berlin, Vols. 40 and 49.